THE JOURNAL OF PHYSICAL CHEMISTRY C

Article

Cite This: J. Phys. Chem. C 2019, 123, 1931−1938

pubs.acs.org/JPCC

Geometric Structures and Electronic Properties of $Al_nV^{0/-}$ (n = 5−14) Clusters: Photoelectron Spectroscopy and Theoretical Calculations

Xinxin Xia,[†,‡] Zeng-Guang Zhang,[§] Hong-Guang Xu,[§] Xiling Xu,[§] Xiaoyu Kuang,*[,†] Cheng Lu,*[,‡,∥] and Weijun Zheng*[,§,⊥]

[†]Institute of Atomic and Molecular Physics, Sichuan University, Chengdu 610065, China

[‡]Department of Physics, Nanyang Normal University, Nanyang 473061, China

[§]Beijing National Laboratory for Molecular Sciences, State Key Laboratory of Molecular Reaction Dynamics, Institute of Chemistry, Chinese Academy of Sciences, Beijing 100190, China

[∥]School of Science, Northwestern Polytechnic University, Xi'an 710072, China

[⊥]University of Chinese Academy of Sciences, Beijing 100049, China

Supporting Information

ABSTRACT: Aluminum and aluminum-doped clusters have gained much attention in cluster science due to their potential applications in nanotechnology. Here, we report a combined photoelectron spectroscopy and density functional theory study of V-doped aluminum clusters. The lowest-energy geometric structures of neutral and anionic $Al_nV^{0/-}$ (n = 5−14) clusters are identified by comparing the theoretical photoelectron spectra with the experimental results. Our results reveal that ground-state structural evolution of neutral and anionic clusters follows different patterns. The V atom in neutral Al_nV clusters moves from convex capped to surface-substituted, to encapsulated site at n = 12, and then returns to surface-substituted sites again. However, as for the anionic Al_nV^-, the metal V atom always occupies the convex capped sites with the cluster size increasing to n = 14. The most stable structure of $Al_{14}V^-$ cluster possesses a C_{3v} symmetric cagelike structure with the highest occupied molecular orbital−lowest unoccupied molecular orbital gap of 1.52 eV. Molecular orbital and adaptive natural density partitioning analysis of $Al_{14}V^-$ suggests that the peripheral Al−Al interactions and delocalized Al−V interactions play important roles in its structural stability.

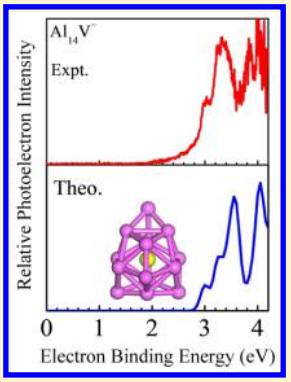

1. INTRODUCTION

The structures and the electronic properties of pure aluminum clusters, different from those of the bulk materials, have attracted intensive research attention in cluster science. Substantial size- and structure-dependent properties of aluminum clusters have been studied.[1−12] Early theoretical studies have indicated that Al_6 and Al_{13} clusters exhibit a clear jellium-type shell structure.[3,4] The size-selected Al_n^- (n = 1−162) clusters have been characterized by photoelectron spectroscopy (PES), and the results showed that the electron shell effect is related with the cluster size.[5] Joint PES and theoretical investigations have shown that the critical size of face-centered cubic-resembling structures to decahedral ones for anionic aluminum clusters occurs at Al_{20}.[7] For Al_n (n < 80) clusters, the ionization potentials have been obtained by photoionization spectroscopy[8] and the structural transition has been observed by density functional theory (DFT) calculation.[9−11] In addition, the structures and the electronic properties of Al_n^+ (n = 3−26) clusters have been studied. The results showed that both structural stability and electronic properties are related to the cluster size.[12]

Metal doping opens a new route to design cluster structures and electronic properties.[13−22] Importantly, metal-doped clusters are expected to have higher structural and electronic stability than bulk materials and pure metal clusters. Several experimental and theoretical studies have explored the structural and electronic properties of aluminum clusters doped with different metal atoms, suggesting that proper doping can enhance the stability of Al_{13} cluster[13] and different atom dopants can remarkably change the structure of the host aluminum cluster.[14−19] Combined PES and DFT research of a series of gold−aluminum alloy clusters showed that the Al−Al interaction plays a more dominant role than the Au−Au interaction in the $Au_xAl_y^-$ ($x + y$ = 7, 8; x = 1−3; y = 4−7)[20] clusters, and the two gold atoms are separated due to the strong interactions between Au and Al in $Au_2Al_n^-$ (n = 3−11) clusters.[21] Very recently, we have systematically investigated the geometric structure, growth behavior, and electronic properties of pure and Mg-doped $Al_n^{0/-}$ (n = 3−20) clusters and found that the ground-state structures of $Al_nMg^{0/-}$ show new structural configuration and evolutionary pattern, in contrast to that of the $Al_n^{0/-}$ clusters.[22]

As most studies indicated, metal doping actually changes the structural configuration and electronic properties and thus

Received: September 14, 2018
Revised: December 29, 2018
Published: December 31, 2018

DOI: 10.1021/acs.jpcc.8b09010
J. Phys. Chem. C 2019, 123, 1931−1938

improved the stability of the host aluminum clusters. However, systematic investigations on V-doped aluminum clusters are relatively scarce, both experimentally and theoretically. V-doped aluminum cation clusters have been reported by combined mass spectrometry and theoretical studies, and the localized position of the V impurity atom gradually changes as a function of cluster size.[23,24] The result showed that, for the lowest-energy structure of Al_nV^+ clusters, the V atom always localizes at the surface site up to $Al_{17}V^+$, beyond which the encapsulated structure arises.[23] To our knowledge, there is no systematic experimental/theoretical research on neutral and anionic Al_nV clusters. Therefore, it is interesting to explore the structural evolution and electronic properties of neutral and anionic V-doped aluminum clusters. Here, we perform photoelectron spectroscopy experiment and theoretical investigation on $Al_nV^{0/-}$ (n = 5−14) clusters.

2. COMPUTATIONAL DETAILS

2.1. Experimental Method. The experiment is performed on a home-built apparatus.[25] The Al_nV^- clusters are generated in the laser vaporization cluster source by laser ablation of a rotating translating disk of aluminum−vanadium mixture with a mole ratio of 8:1. Helium gas expands into the source through a pulsed valve to cool the produced clusters under about 0.4 MPa. The mass spectra of the generated cluster anions are measured with a time-of-flight mass spectrometer. The size of anionic Al_nV^- (n = 5−14) clusters is selected with a mass gate, which is decelerated by a momentum decelerator and crossed with a laser beam of another nanosecond Nd:YAG laser. The kinetic energies of the electrons from photodetachment are analyzed by a magnetic bottle photoelectron spectrometer. The spectral resolution of the magnetic bottle photoelectron spectrometer is estimated to be 40 meV. On the basis of the similar experimental conditions, the photoelectron spectra are calibrated with the spectrum of Cu^-.

2.2. Theoretical Method. The unbiased Crystal structure AnaLYsis by Particle Swarm Optimization (CALYPSO) structure searching method[26−28] is used to search the ground-state structures of neutral and anionic V-doped aluminum clusters. The details of this method can be found in previous publications of various systems.[29−36] To achieve convergence around the lowest minima of the potential energy surfaces, we have performed global structure searches at the B3PW91[37−39]/Al/V/3-21G level of theory and obtained 1000−1500 isomers for low-energy anionic and neutral V-doped aluminum clusters based on 30 generations searching. Among these isomers, the top 20 energetically lowest-lying isomers are selected and reoptimized using the B3PW91/6-311+g(d) level as implemented in the Gaussian 09 program package.[40] The calculated results indicate that the energy orders of the top 20 selected isomers obtained are almost the same by using two different calculation levels. During the structure optimization, all possible spin states are considered and no symmetry constraints are imposed. For each isomer, harmonic vibrational frequency analysis is performed to ensure that the structure is a truly local minimum. The photoelectron spectra of Al_nV^- (n = 5−14) clusters are simulated using the time-dependent DFT method. The chemical bonding analysis is conducted using the adaptive natural density partitioning (AdNDP) method.[41]

3. RESULTS AND DISCUSSION

3.1. Experimental Results. The experimental PES of Al_nV^- (n = 5−14) anions recorded at 266 nm wavelength are displayed in Figure 1. The experimental VDEs are obtained

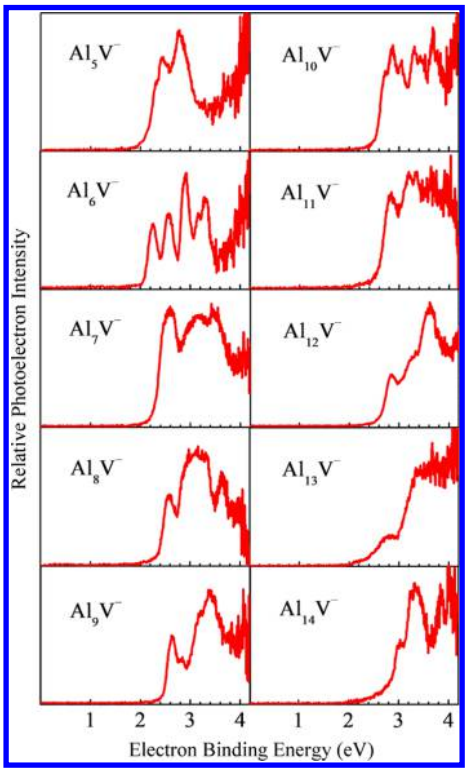

Figure 1. Experimental PES of $Al_nV^{0/-}$ (n = 5−14) clusters.

from the binding energy of the first peaks in the experimental spectra of Al_nV^-. The experimental ADEs are determined by adding the instrumental resolution to the electron binding energies at the crossing point between the baseline and the rising edge of the first peak. The data of the experimental VDEs and experimental ADEs are presented and compared to the theoretical values calculated at the B3PW91/6-311+g(d) level in Table 1.

The spectrum of Al_5V^- has a shoulder at about 2.31 eV and two strong peaks at 2.43 and 2.79 eV. The onset of a broad feature can also be observed above 3.5 eV. The spectrum of Al_6V^- shows five sharp peaks at 2.26, 2.57, 2.91, 3.17, and 3.30 eV. In the spectrum of Al_6V^-, there is also a feature of low signal-to-noise ratio above 3.80 eV. Al_7V^- has a distinct peak centered at 2.59 eV and two unresolved broad features centered at ∼3.14 and 3.46 eV. Al_8V^- has three major peaks from 2.57 to 3.64 eV, during which a broad feature occurs between 2.70 and 3.50 eV. Al_9V^- has a weak peak centered at 2.64 eV, a shoulder peak at 2.83 eV, and a strong unresolved broad feature between 2.90 and 3.50 eV.

$Al_{10}V^-$ has a shoulder peak at 2.72 eV, several other peaks at 2.87, 3.05, 3.31, 3.45, and 3.67 eV, and another peak above 4.00 eV. $Al_{11}V^-$ has a peak centered at 2.83 eV and a strong unresolved broad feature extending from 3.00 to 4.20 eV. $Al_{12}V^-$ has four peaks centered at 2.86, 3.20, 3.34, and 3.62 eV. The front part of another peak is observed above 4.00 eV. The spectrum of $Al_{13}V^-$ shows a tail from 2.00 to 2.60 eV, a small broad peak at 2.80 eV, and a strong broad feature above 3.00 eV. $Al_{14}V^-$ shows a small peak at 3.03 eV and a broad feature

DOI: 10.1021/acs.jpcc.8b09010
J. Phys. Chem. C 2019, 123, 1931−1938

Table 1. Data of Experimental and Theoretical VDEs and ADEs as well as the Electronic States and ΔE of the Al_nV^- (n = 5−14) Clusters and Their Corresponding Low-Lying Isomers[a]

				VDE		ADE	
	isomer	sta.	ΔE	expt.	theo.	expt.	theo.
Al_5V^-	5a$^-$	^{4}A′	0.00	2.31	2.17	2.13	1.83
	5b$^-$	^{6}A′	0.24		1.90		1.78
	5c$^-$	^{4}A″	0.28		1.83		1.68
Al_6V^-	6a$^-$	$^5A_1$	0.00	2.26	2.12	2.10	1.90
	6b$^-$	^{5}A	0.69		2.40		2.10
	6c$^-$	^{1}A′	0.74		1.60		1.80
Al_7V^-	7a$^-$	^{4}A	0.00	2.59	2.35	2.25	2.11
	7b$^-$	^{6}A′	0.05		2.25		1.84
	7c$^-$	^{4}A	0.30		2.20		1.99
Al_8V^-	8a$^-$	^{5}A	0.00	2.57	2.62	2.38	2.42
	8b$^-$	^{3}A	0.02		2.60		2.32
	8c$^-$	^{5}A	0.45		2.35		2.15
Al_9V^-	9a$^-$	^{4}A′	0.00	2.64	2.49	2.49	2.30
	9b$^-$	^{4}A″	0.25		2.80		2.60
	9c$^-$	^{4}A	0.50		3.05		2.42
$Al_{10}V^-$	10a$^-$	^{3}A″	0.00	2.72	2.48	2.56	2.35
	10b$^-$	^{3}A	0.30		3.10		2.80
	10c$^-$	^{1}A′	1.55		1.60		1.44
$Al_{11}V^-$	11a$^-$	^{4}A	0.00	2.83	2.60	2.59	2.41
	11b$^-$	^{6}A′	0.23		2.55		2.30
	11c$^-$	^{4}A	0.50		2.75		2.60
$Al_{12}V^-$	12a$^-$	^{3}A′	0.00	2.86	2.79	2.60	2.51
	12b$^-$	^{3}A	0.16		2.95		2.72
	12c$^-$	^{3}A′	0.59		3.30		2.70
$Al_{13}V^-$	13a$^-$	^{6}A′	0.00	2.80	2.05	2.36	2.01
	13b$^-$	^{6}A′	0.19		3.00		2.40
	13c$^-$	^{4}A″	1.70		2.80		2.62
$Al_{14}V^-$	14a$^-$	$^3A_1$	0.00	3.03	3.00	2.84	2.82
	14b$^-$	^{5}A′	0.04		2.50		2.26
	14c$^-$	^{1}A	1.21		2.45		2.24

[a]All energies are in eV.

between 3.10 and 3.60 eV. In addition, two peaks of low signal-to-noise ratio can also be observed at ∼3.83 and 4.00 eV.

3.2. Theoretical Results. The lowest-energy structures and the key low-lying isomers of Al_nV^- (n = 5−14) clusters are presented in Figure 2. To further study the geometric properties, we simulate their photoelectron spectra and compare the results with experimental PES (Figure 3). In addition, the relative energies (ΔE) of the low-lying isomers and the calculated VDEs and ADEs of anions are displayed in Table 1 and compared to the experimental data.

3.2.1. Al_nV^- (n = 5−14) Anions. 3.2.1.1. Al_5V^-. The most stable structure of Al_5V^-, 5a$^-$, can be considered as adding a face-capping V atom to Al_5 cluster.[22] The calculated VDE is very close to the experimental result. The spectrum of 5a$^-$ can roughly reproduce the experimental peak positions, although the overall spectrum is a little narrower and is moved to lower binding energy. In the low-lying isomer (5b$^-$) of Al_5V^-, five Al atoms constitute a pentahedron and the V atom locates at the bottom, forming a bottom-capped octahedron. The energy of 5b$^-$ is 0.24 eV higher than that of 5a$^-$. The ADE and VDE of 5c$^-$ are 1.68 and 1.83 eV, which have relatively large discrepancy with the experimental values. Therefore, it seems that the most stable structure of 5a$^-$ is the most likely structure detected in the experimental spectrum.

3.2.1.2. Al_6V^-. As the ground-state structure of Al_6V^-, 6a$^-$ can be considered as an Al_6 triangular prism face-capped by a V atom. The theoretical VDE of 6a$^-$ agrees well with the experimental result, and its theoretical spectrum matches well with the experimental one. Isomer 6b$^-$ is formed by adding an Al atom to side-cap the ground-state structure of 5a$^-$. Although both the theoretical VDE and ADE of 6b$^-$ are close to the experimental data, the existence of 6b$^-$ can be excluded because it is much less stable than isomer 6a$^-$. For isomer 6c$^-$, it can be ruled out in our experiments because it is higher in energy than isomer 6a$^-$ by 0.74 eV. Therefore, isomer 6a$^-$ makes the main contribution to our experiments.

3.2.1.3. Al_7V^-. The most stable isomer of Al_7V^- (7a$^-$) is of C_1 symmetry, in which all of the atoms form a 1-4-3 layered structure.[42] The calculated VDE (2.35 eV) of isomer 7a$^-$ is slightly lower than the experimental value (2.60 eV), but the spectrum features for simulated and experimental PES match very well. Isomer 7b$^-$ can be viewed as an Al atom face-capping the low-lying structure of Al_6V^- (6c$^-$). The energy is only 0.05 eV higher than that of 7a$^-$. The theoretical VDE (2.25 eV) of isomer 7b$^-$ is a little lower than the experimental result, but there are two peaks of the simulated spectrum in excellent agreement with the experimental peaks centered at 2.60 and 3.05 eV. For isomer 7c$^-$, the structure is similar to that of isomer 7a$^-$, while its energy is 0.30 eV higher than that of 7a$^-$. Therefore, both isomers 7a$^-$ and 7b$^-$ contribute to our experimental spectrum.

3.2.1.4. Al_8V^-. The lowest-energy structure of Al_8V^- (8a$^-$) can be viewed as a cagelike structure with the doped V atoms at the bottom. The low-lying isomer (8b$^-$) can be obtained by an additional Al atom capping the triangular face of 7b$^-$. The VDEs of 8a$^-$ and 8b$^-$ are 2.62 and 2.60 eV, respectively, both of which are consistent with the experimental result (2.58 eV). Compared to experiment, the overall spectrum of 8a$^-$ moves backward in binding energy and reproduces the peak positions and patterns. Meanwhile, two peaks of the simulated spectrum of isomer 8b$^-$ are in good agreement with the experimental peaks at 2.60 and 3.30 eV. Isomer 8c$^-$ is impossible to be observed in the experimental spectrum because it is higher in energy than 8a$^-$ by 0.45 eV. Thus, both isomers 8a$^-$ and 8b$^-$ make important contribution to the experiments.

3.2.1.5. Al_9V^-. In the ground-state structure of Al_9V^- (9a$^-$), nine Al atoms constitute a semienclosed cagelike structure and one V atom fills in the projecting position, forming a face-capped cagelike structure. Both isomers 9b$^-$ and 9c$^-$ have prolate structures, which are 0.25 and 0.50 eV higher in energy than 9a$^-$, respectively. In the simulated spectrum of 9a$^-$, both the VDE and ADE are in reasonable agreement with experimental resutes. Besides, the essential characteristics and trends of experimental spectrum are excellently reproduced by theoretical spectrum. Therefore, the isomer 9a$^-$ is the major one detected in our experiments.

3.2.1.6. $Al_{10}V^-$. The most stable isomer 10a$^-$ follows the structural motif of 9a$^-$, which can be viewed as capping one Al atom inside the Al_4 diamond of 9a$^-$. Adding one Al_3 unit inside the isomer 7c$^-$ leads to the 10b$^-$. Isomer 10c$^-$ can be seen as capping an Al atom on 9a$^-$ with some reconstruction. The calculated VDE of 10a$^-$ is slightly lower than the experimental value. In the simulated spectrum of 10a$^-$, the first two peaks moved forward in binding energy while the overall spectral characteristics are consistent with the experimental trend. The

DOI: 10.1021/acs.jpcc.8b09010
J. Phys. Chem. C 2019, 123, 1931−1938

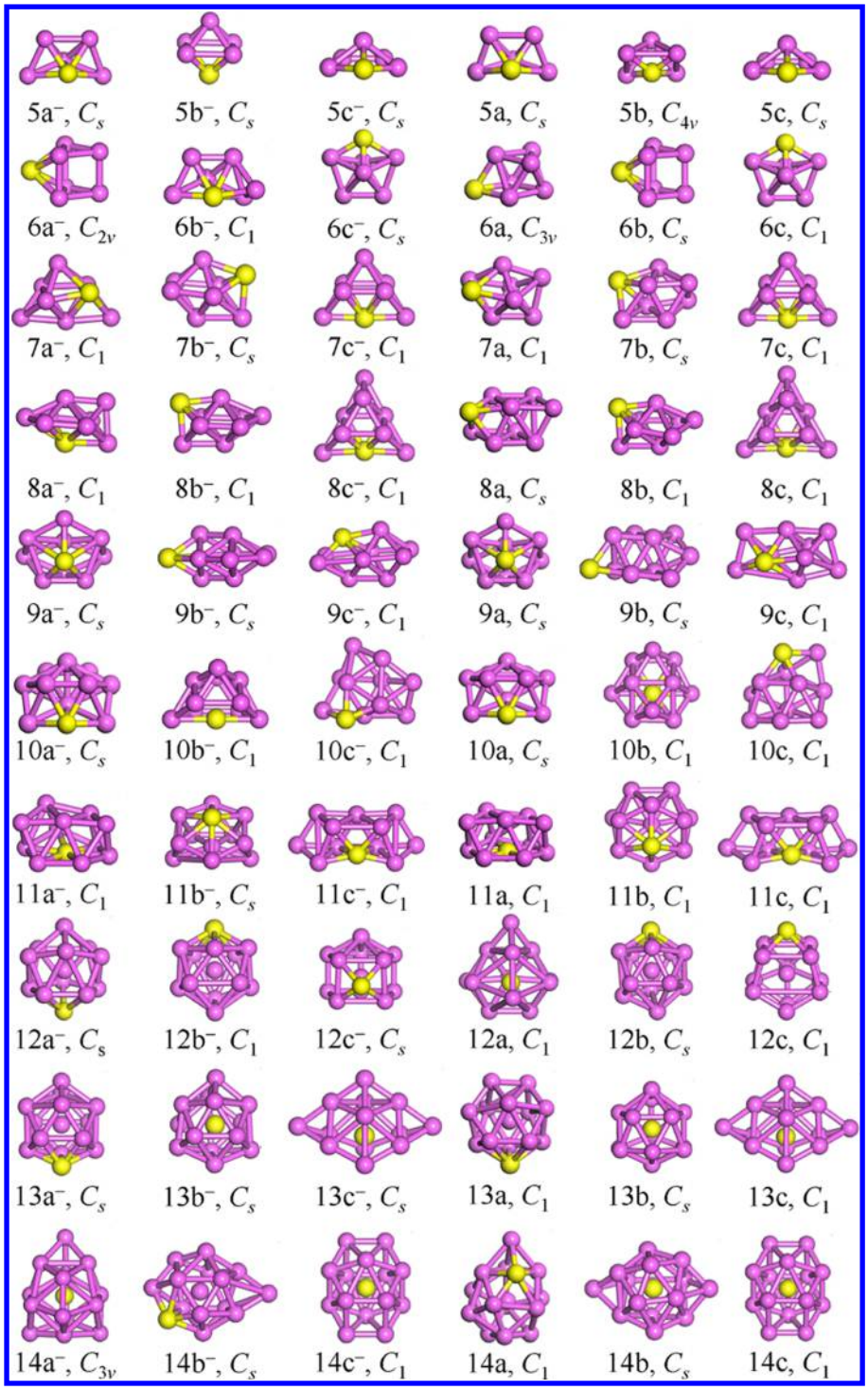

Figure 2. Geometrical structures of the ground-state and low-lying isomers of $Al_nV^{0/-}$ (n = 5−14) clusters. The pink (yellow) spheres represent the Al (V) atoms.

simulated spectrum of 10c⁻ is consistent with the experimental characteristic centered at 3.00 and 3.30 eV. The existence of isomer 10b⁻ can be ruled out by comparing the simulated spectrum and the experimental one. Thus, isomer 10a⁻ is the main one observed in our experiments and isomer 10c⁻ less possibly contributes to the experimental spectrum of $Al_{10}V^-$.

3.2.1.7. $Al_{11}V^-$. In the ground-state structure of $Al_{11}V^-$ (11a⁻), the V atom tends to move inside the caged aluminum framework. The location of V atom is still in the surface of 11b⁻. For isomer 11c⁻, the V atom is already sunken. Isomer 11c⁻, which is 0.50 eV higher in energy than 11a⁻, can be viewed as an Al atom capping on the most stable isomer of 10a⁻. The theoretical VDEs of isomers 11a⁻ and 11b⁻ (2.60 and 2.55 eV) are consistent with the experimental value (2.83 eV). Also, the simulated spectrum of 11a⁻ shows a similar trend to the experimental peak in the range of 3.56−3.79 eV, and the simulated spectrum of isomer 11b⁻ is in reasonable agreement with the experimental peak in 2.83 eV. From the calculated spectra of $Al_{11}V^-$, it is possible that both isomers 11a⁻ and 11b⁻ contribute to our experimental spectrum.

DOI: 10.1021/acs.jpcc.8b09010
J. Phys. Chem. C 2019, 123, 1931−1938

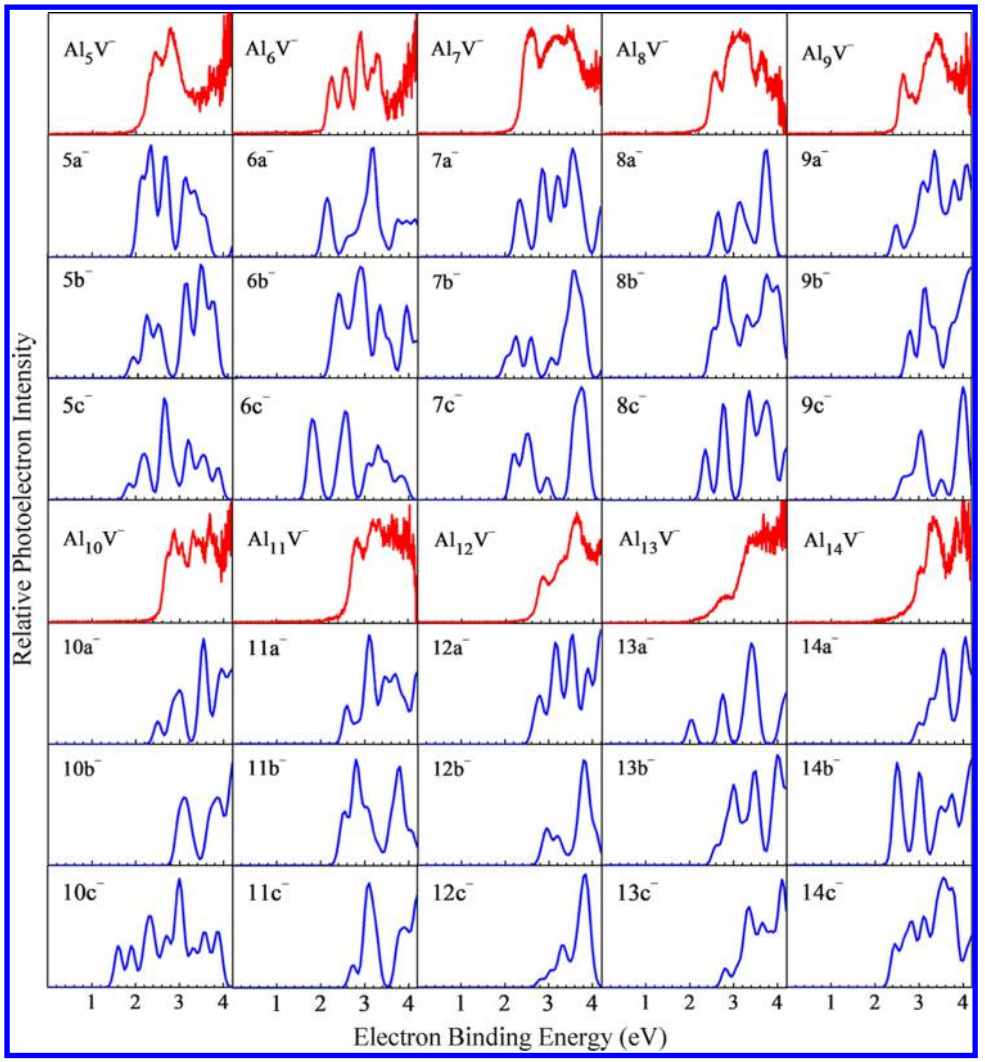

Figure 3. Experimental and simulated PES of Al_nV^- (n = 5−14) clusters.

Multiple isomers coexisting in the experimental result give the reason why the spectral feature of $Al_{11}V^-$ is relatively broad.

3.2.1.8. $Al_{12}V^-$. Isomer 12a$^-$ has a C_s symmetric cagelike structure with one Al atom encapsulated inside the cage of 10a$^-$ and another Al atom capping the top of 10a$^-$ with some reconstruction. The structure of isomer 12b$^-$ is similar to that of 12a$^-$, but it is less stable than isomer 12a$^-$ by 0.16 eV. Isomer 12c$^-$ with C_s symmetry is higher in energy than isomer 12a$^-$ by 0.59 eV. Therefore, 12c$^-$ is improbable to be observed in the experimental spectrum. The experimental VDE (2.86 eV) is excellently reproduced by the calculated VDEs (2.79 and 2.95 eV, respectively) of 12a$^-$ and 12b$^-$. In addition, the experimental trend is successfully simulated by the theoretical PES of 12a$^-$. According to the analysis, we can conclude that both 12a$^-$ and 12b$^-$ contribute to the experimental spectrum of $Al_{12}V^-$.

3.2.1.9. $Al_{13}V^-$. As the lowest-energy isomer, 13a$^-$ is constructed by doping an Al atom on the face of 12a$^-$. For 13b$^-$ and 13c$^-$ isomers, the V atom is fully encapsulated in the aluminum framework. The calculated VDE of isomer 13b$^-$ is 3.00 eV, very close to the experimental value (2.83 eV). The energy of isomers 13b$^-$ is only 0.19 eV higher than that of 13a$^-$. Therefore, 13b$^-$ is the most probable structure for $Al_{13}V^-$ detected from the experimental PES. For isomer 13a$^-$, the VDE (2.05 eV) is much lower than that of the experimental value. Isomer 13c$^-$ also can be ruled out, which is much higher in energy than 13a$^-$.

3.2.1.10. $Al_{14}V^-$. The most stable isomer $Al_{14}V^-$ (14a$^-$) is a C_{3v} symmetric cagelike structure with one V atom encapsulated inside the Al_{14} cage. The isomer 14b$^-$ can be regarded as adding an Al atom to the top of 13a$^-$. The theoretical VDE (3.00 eV) of isomer 14a$^-$ excellently repeats the experimental value (3.03 eV). In addition, its theoretical spectrum successfully reproduces the experimental peaks and presents the same tendency with the experimental one. Although the energy of isomer 14b$^-$ is only slightly higher than that of 14a$^-$, the theoretical VDE (2.50 eV) is much lower than our experimental value (3.03 eV). Thus, isomer 14b$^-$ is unlikely to be observed in the experiments. Meanwhile, isomer 14c$^-$ can be ruled out because its energy is 1.21 eV higher than that of 14a$^-$. Therefore, we suggest that isomer 14a$^-$ is the major one observed in the experiment. As described above, we can see a reasonable agreement between theoretical and experimental photoelectron spectra, demonstrating the reliability of the present computational results.

3.2.2. Al_nV (n = 5−14) Neutrals. The ground-state structures and some typical low-lying isomers of neutral Al_nV (n = 5−14) clusters are displayed in Figure 2 with the corresponding anions for comparison. In addition, the electronic states and ΔE of them are also listed in Table S1.

DOI: 10.1021/acs.jpcc.8b09010
J. Phys. Chem. C 2019, 123, 1931−1938

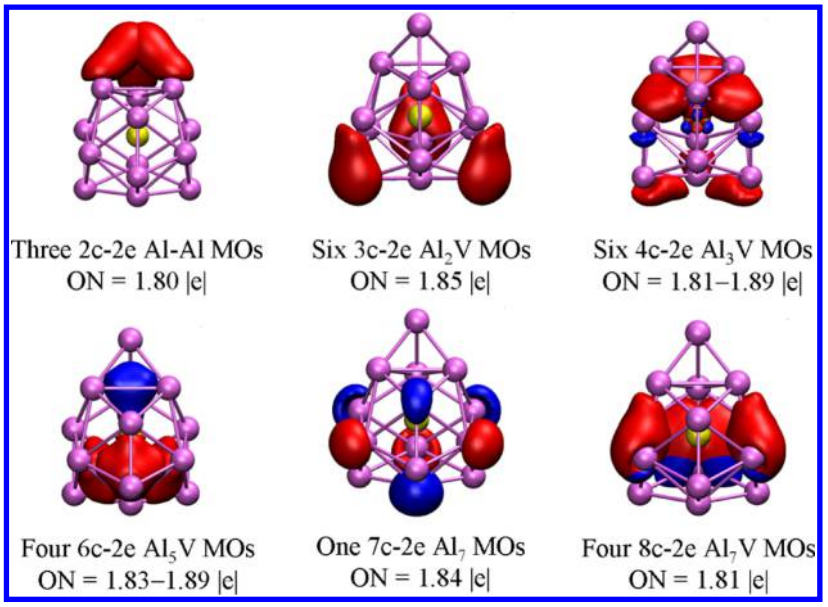

Figure 4. Chemical bonding of anionic $Al_{14}V^-$ cluster. ON is the occupation number.

From Figure 2, we can find that the ground-state structures of $Al_{6,7,8,12,14}V$ clusters are different from those of the corresponding anions. The lowest-energy structure of Al_6V is analogous to that of anion 6a$^-$ with a slight distortion of top triangle. The ground state of Al_7V, 7a, is obtained by adding one V atom to cap one angle of Al_6V, forming a starfish structure. The ground-state structure (8a) of Al_8V can be viewed as a slant four-prism capped with one V atom on the left-hand side. As for $Al_{12}V$, the ground-state structure (12a) can be seen as a doped V atom encapsulated by the caged aluminum framework. The most stable isomer (14a) of $Al_{14}V$ can be described as a caged aluminum cluster capped with an additional Al atom and a doped V atom on either sides. For the neutral low-lying isomers, except for 5b, 10b, and 12c, the structure and energy sequences are similar to those of Al_nV^- anions with slight difference in symmetries. Isomer 5b is a C_{4v} symmetric pyramid structure with the V atom located at the bottom. The low-lying isomer 10b is a cagelike structure, which can be viewed as adding a V atom to the surface of the structure. As for $Al_{12}V$, the low-lying isomer 12c is an encapsulated structure with the V atom adding to the top of the Al_{12} cluster.

3.3. Discussion. The theoretical results described above show that the structural evolution of the neutral Al_nV clusters is somewhat different from their anions. For anions, the V atom in the ground-state structures is invariably inclined to stay in the convex capping position when $n \leq 11$. With the size of clusters increasing, a significant structural transformation is observed at the $Al_{14}V^-$ cluster, in which the V atom occupies the center site to form an encapsulated structure. However, the first encapsulated structure of anionic low-lying structures occurs at $n = 13$. For neutral Al_nV clusters, the occupied position of the V atom in ground-state structures moves from the convex capping position when $n \leq 10$ to the surface-doped position when $n = 11$, and subsequently to the encapsulated state when $n = 12$ and to the convex capping position again when n reached 13 and 14. In short, the cage configuration appears at $n = 14$ for anions. However, for neutral clusters, the metal V atom encapsulation of Al_n cage can be achieved at $n = 12$. In addition to the different structural evolution patterns, we obtain that the ground-state structures of Al_nV^- (n = 6, 8, 12, 13, 14) clusters are different from those of the corresponding neutral ones, that is, the extra electron would affect the geometric structures of Al_nV clusters.

To confirm that the dopants can induce novel geometric structures and different structural evolution patterns, we make a detailed comparison of the structures of the $Al_nV^{0/-}$, $MgAl_n^{0/-}$ ($n = 3-20$), and pure $Al_n^{0/-}$ ($n = 3-20$) clusters.[22] For the pure $Al_n^{0/-}$ ($n = 5-14$) clusters, only the ground-state structure of the $Al_5^{0/-}$ cluster is planar, and the neutral and anionic $Al_n^{0/-}$ ($6 \leq n \leq 14$) clusters all have three-dimensional cagelike structures. However, the ground-state structures of both $Al_nV^{0/-}$ and $MgAl_n^{0/-}$ clusters are stereoscopic. The structural analysis results show that both $Al_nV^{0/-}$ and $MgAl_n^{0/-}$ clusters with $5 \leq n \leq 8$ always form the exohedral-doped structures by attaching or substituting the atom of host aluminum clusters, but the most stable structures of $Al_{9,10,11}V^{0/-}$ clusters are slightly different from those of either Al_n units or $MgAl_n^{0/-}$ clusters. The structural evolution of $MgAl_n^{0/-}$ clusters shows that the doped Mg atom prefers to stay at the convex capping position and no encapsulated structure has been found from $n = 3$ to 20. For neutral Al_nV clusters, the endohedral structure starts to form from $n = 11$ and the V atom is totally encapsulated in an aluminum cage at $n = 12$, while encapsulated structures for anions occur at $n = 14$. This clearly implies that different dopants not only influence the structural properties of the host aluminum clusters but also follow different structural evolution patterns. Previous papers[43,44] have pointed out that the critical size of the cagelike structure is always related to the radius of doped atom. The bigger the doped atom is, the bigger host cluster is needed. The radius of V atom is larger than that of Mg, but the smallest cagelike structure of $Al_nV^{0/-}$ clusters forms before $MgAl_n^{0/-}$ clusters. However, the neutral Al_nV and VSi_n clusters[45] form the smallest cagelike structure at the same size $n = 12$. The bonding of $MgAl_n^{0/-}$ clusters is dominated by the *s* electrons of Mg atom and the *p* electron of Al atoms, corresponding to *sp* hybridization. However, the bonding of $Al_nV^{0/-}$ and VSi_n clusters, corresponding to *pd* hybridization, is formed primarily by the *d* electrons of V atom and the *p* electron of Al (Si) atoms. So, on the basis of the above

DOI: 10.1021/acs.jpcc.8b09010
J. Phys. Chem. C 2019, 123, 1931−1938

discussions, we can deduce that the reason why $Al_nV^{0/-}$ and $MgAl_n^{0/-}$ clusters form cagelike structures at different sizes can be explained by the bonding properties and orbital hybridization between the doped atom and Al atoms.

The average binding energy (E_b) of $Al_nV^{0/-}$ (n = 5−14) clusters is displayed in Figure S1a, which is a useful measure of inherent stability. To investigate the chemical bonding properties of V-doped aluminum clusters, we analyzed their molecular orbitals (MOs). For simplicity, we just present the results of $Al_{14}V^-$ cluster, which have higher stability and larger highest occupied molecular orbital−lowest unoccupied molecular orbital (HOMO−LUMO) energy gap (1.52 eV) than other clusters (see Figure S1b). The bonding interactions can be seen from MOs in Figure S2, where the interactions between the central V and the peripheral Al atoms are strong and make the C_{3v} structure of $Al_{14}V^-$ more stable. To get an in-depth understanding of the bonding nature, the chemical bonding in $Al_{14}V^-$ cluster is also analyzed using the AdNDP method and is presented in Figure 4, which yields two different types of bonds (localized and delocalized bonds). The total valence electron numbers of the $Al_{14}V^-$ anion is 48, which includes 42 valence electrons of the 14 Al atoms, 5 valence electrons of the V atom, and an excess electron. From Figure 4, we can see that there are only three 2c−2e localized Al−Al σ bonds, which include six valence electrons of the $Al_{14}V^-$ anion. The remaining 42 valence electrons are occupied by the additional 21 delocalized $Al_{14}V^-$ bonds. The delocalized bonds include six 3c−2e bonds, six 4c−2e bonds, four 6c−2e bonds, one 7c−2e bond, and four 8c−2e bonds. The occupation number (ON) of the 2c−2e bonds is 1.81|e|, suggesting little interaction with the central V atom. The six 3c−2e bonds with ON = 1.85|e| represent the interactions between the six localized σ bonds and the central V atom, while the six 4c−2e delocalized σ bonds with ON = 1.81−1.89|e|, three of which are 1.81|e| and the other three are 1.89|e|, represent the bonding in each Al_3 unit and the central V atom. The four 6c−2e bonds, where ON = 1.83−1.89|e|, are mainly formed by bonding the peripheral Al_5 units and the central V atom. There is only one 7c−2e σ bond, shown in Figure 4, representing bonding interactions among seven Al atoms. For the 8c−2e Al_7V MOs, the bonding interactions between the peripheral Al_7 units and the central V atom may lead to its high electronic stability. According to the above analysis, we can see that both the Al−Al bonds and the Al−V bonds are important for the substantial stabilization of the C_{3v} symmetric structure of $Al_{14}V^-$ anion.

4. CONCLUSIONS

In conclusion, we have presented a joint photoelectron spectroscopy experiment and theoretical investigation on the structural and electronic properties of neutral and anionic $Al_nV^{0/-}$ (n = 5−14) clusters. The ground-state structures of $Al_nV^{0/-}$ (n = 5−14) clusters are determined by an unbiased CALYPSO structure searching method. It is found that the neutral and anionic Al_nV clusters show different structural evolution patterns. The V atom in neutral Al_nV moves from convex capped to surface-substituted, to encapsulated site at n = 12, and then returns to surface-substituted sites again. However, as for the anionic Al_nV^-, the metal V atom always occupies the convex capped sites with the cluster size increasing to n = 14. These results indicate that an extra electron visibly affects the geometric structures of Al_nV clusters. Most remarkable is that the $Al_{14}V^-$ cluster shows superior stability with a C_{3v} cagelike structure and a large HOMO−LUMO gap. The present results provide us a complete picture of the structural evolution on V-doped aluminum clusters, with a hope that it can offer valuable information for further experimental and theoretical studies.

■ ASSOCIATED CONTENT

Supporting Information

The Supporting Information is available free of charge on the ACS Publications website at DOI: 10.1021/acs.jpcc.8b09010.

Size dependence of the average binding energies and HOMO−LUMO energy gaps of $Al_nV^{0/-}$ (n = 5−14) clusters (Figure S1); molecular orbitals of anionic $Al_{14}V^-$ cluster (Figure S2); and the electronic states and relative energies (ΔE) of neutral Al_nV (n = 5−14) clusters and their corresponding low-lying isomers (Table S1) (PDF)

■ AUTHOR INFORMATION

Corresponding Authors

*E-mail: scu_kuang@163.com. Tel: +86-028-85403803 (X.K.).
*E-mail: lucheng@calypso.cn. Tel: +86-0377-63513721 (C.L.).
*E-mail: zhengwj@iccas.ac.cn. Tel: +86-010-62635054 (W.Z.).

ORCID

Xiaoyu Kuang: 0000-0001-7489-9715
Cheng Lu: 0000-0003-1746-7697
Weijun Zheng: 0000-0002-9136-2693

Notes

The authors declare no competing financial interest.

■ ACKNOWLEDGMENTS

This work was supported by the National Natural Science Foundation of China (Nos. 11574220, 11874043, 21671114, and U1804121).

■ REFERENCES

(1) Upton, T. H. Structural, Electronic, and Chemisorption Properties of Small Aluminum Clusters. *Phys. Rev. Lett.* **1986**, *56*, 2168−2171.
(2) Douglas-Gallardo, O. A.; Soldano, G. J.; Mariscal, M. M.; Sánchez, C. G. Effects of Oxidation on the Plasmonic Properties of Aluminum Nanoclusters. *Nanoscale* **2017**, *9*, 17471−17480.
(3) Akola, J.; Häkkinen, H.; Manninen, M. Ionization Potential of Aluminum Clusters. *Phys. Rev. B* **1998**, *58*, 3601−3604.
(4) Sengupta, T.; Das, S.; Pal, S. Oxidative Addition of the C-I Bond on Aluminum Nanoclusters. *Nanoscale* **2015**, *7*, 12109−12125.
(5) Li, X.; Wu, H. B.; Wang, X. B.; Wang, L. S. *s*−*p* Hybridization and Electron Shell Structures in Aluminum Clusters: A Photoelectron Spectroscopy Study. *Phys. Rev. Lett.* **1998**, *81*, 1909−1912.
(6) Akola, J.; Manninen, M.; Häkkinen, H.; Landman, U.; Li, X.; Wang, L. S. Photoelectron Spectra of Aluminum Cluster Anions: Temperature Effects and Ab Initio Simulations. *Phys. Rev. B* **1999**, *60*, No. R11297.
(7) Akola, J.; Manninen, M.; Häkkinen, H.; Landman, U.; Li, X.; Wang, L. S. Aluminum Cluster Anions: Photoelectron Spectroscopy and Ab Initio Simulations. *Phys. Rev. B* **2000**, *62*, 13216−13228.
(8) Cândido, L.; Rabelo, J. N. T.; Da Silva, J. L. F.; Hai, G. Q. Quantum Monte Carlo Study of Small Aluminum Clusters Al_n (n = 2-13). *Phys. Rev. B* **2012**, *85*, No. 245404.

DOI: 10.1021/acs.jpcc.8b09010
J. Phys. Chem. C 2019, 123, 1931−1938

(9) Schriver, K. E.; Persson, J. L.; Honea, E. C.; Whetten, R. L. Electronic Shell Structure of Group-IIIA Metal Atomic Clusters. *Phys. Rev. Lett.* **1990**, *64*, 2539−2542.
(10) Chuang, F. C.; Wang, C. Z.; Ho, K. H. Structure of Neutral Aluminum Clusters Al_n ($2 \leq n \leq 23$): Genetic Algorithm tight-binding calculations. *Phys. Rev. B* **2006**, *73*, No. 125431.
(11) Rao, B. K.; Jena, P. Evolution of the Electronic Structure and Properties of Neutral and Charged Aluminum Clusters: A Comprehensive Analysis. *J. Chem. Phys.* **1999**, *111*, 1890−1904.
(12) Jarrold, M. F.; Bower, J. E.; Kraus, J. S. Collision Induced Dissociation of Metal Cluster Ions: Bare Aluminum Clusters, Al_n^+(n = 3−26). *J. Chem. Phys.* **1987**, *86*, 3876.
(13) Gong, X. G.; Kumar, V. Enhanced Stability of Magic Clusters: A Case Study of Icosahedral $Al_{12}X$, X = B, Al, Ga, C, Si, Ge, Ti, As. *Phys. Rev. Lett.* **1993**, *70*, 2078−2081.
(14) Li, S. F.; Gong, X. G. Neutral and Negatively Charged $Al_{14}X$ (X = Si, Ge, Sn, Pb) Clusters Studied from First Principles. *Phys. Rev. B* **2006**, *74*, No. 045432.
(15) Kumar, V.; Sundararajan, V. Ab Initio Molecular-Dynamics Studies of Doped Magic Clusters and Their Interaction with Atoms. *Phys. Rev. B* **1998**, *57*, 4939−4942.
(16) Calleja, M.; Rey, C.; Alemany, M. M. G.; Gallego, L. J.; Ordejón, P.; Sánchez-Portal, D.; Artacho, E.; Soler, J. M. Self-Consistent Density-Functional Calculations of the Geometries, Electronic Structures, and Magnetic Moments of Ni-Al Clusters. *Phys. Rev. B* **1999**, *60*, 2020−2024.
(17) Zope, R. R.; Baruah, T. Conformers of Al_{13}, $Al_{12}M$, and $Al_{13}M$ (M = Cu, Ag, and Au) Clusters and Their Energetics. *Phys. Rev. A* **2001**, *64*, No. 053202.
(18) Rexer, E. F.; Jellinek, J.; Krissinel, E. B.; Parks, E. K.; Riley, S. J. Theoretical and Experimental Studies of the Structures of 12-, 13-, and 14-Atom Bimetallic Nickel/Aluminum Clusters. *J. Chem. Phys.* **2002**, *117*, 82−94.
(19) Pal, R.; Cui, L. F.; Bulusu, S.; Zhai, H. J.; Wang, L. S.; Zeng, X. C. Probing the Electronic and Structural Properties of Doped Aluminum Clusters: MAl_{12}^- (M = Li, Cu, and Au). *J. Chem. Phys.* **2008**, *128*, No. 024305.
(20) Khetrapal, N. S.; Jian, T.; Pal, R.; Lopez, G. V.; Pande, S.; Wang, L. S.; Zeng, X. C. Probing the Structures of Gold-Aluminum Alloy Clusters $Au_xAl_y^-$: A Joint Experimental and Theoretical Study. *Nanoscale* **2016**, *8*, 9805.
(21) Khetrapal, N. S.; Jian, T.; Lopez, G. V.; Pande, S.; Wang, L. S.; Zeng, X. C. Probing the Structural Evolution of Gold-Aluminum Bimetallic Clusters ($Au_2Al_n^-$, n = 3−11) Using Photoelectron Spectroscopy and Theoretical Calculations. *J. Phys. Chem. C* **2017**, *121*, 18234−18243.
(22) Xing, X. D.; Wang, J. J.; Kuang, X. Y.; Xia, X. X.; Lu, C.; Maroulis, G. Probing the Low-Energy Structures of Aluminum-Magnesium Alloy Clusters: A Detailed Study. *Phys. Chem. Chem. Phys.* **2016**, *18*, 26177−26183.
(23) Fernández, E. M.; Vega, A.; Balbás, L. C. Theoretical Study of Al_n V^+ Clusters and Their Interaction with Ar. *J. Chem. Phys.* **2013**, *139*, No. 214305.
(24) Vanbuel, J.; Fernández, E. M.; Ferrari, P.; Gewinner, S.; Schöllkopf, W.; Balbás, L. C.; Fielicke, A.; Janssens, E. Hydrogen Chemisorption on Singly Vanadium-Doped Aluminum Clusters. *Chem. - Eur. J.* **2017**, *23*, 15638−15643.
(25) Xu, H. G.; Zhang, Z. G.; Feng, Y.; Yuan, J. Y.; Zhao, Y. C.; Zheng, W. J. Vanadium-Doped Small Silicon Clusters: Photoelectron Spectroscopy and Density-Functional Calculations. *Chem. Phys. Lett.* **2010**, *487*, 204−208.
(26) Wang, Y. C.; Lv, J.; Zhu, L.; Ma, Y. M. CALYPSO: A Method for Crystal Structure Prediction. *Comput. Phys. Commun.* **2012**, *183*, 2063−2070.
(27) Lv, J.; Wang, Y. C.; Zhu, L.; Ma, Y. M. Particle-Swarm Structure Prediction on Clusters. *J. Chem. Phys.* **2012**, *137*, No. 084104.
(28) Wang, Y. C.; Lv, J.; Zhu, L.; Ma, Y. M. Crystal Structure Prediction via Particle-Swarm Optimization. *Phys. Rev. B* **2010**, *82*, No. 094116.
(29) Zhu, L.; Liu, H. Y.; Pickard, C. J.; Zou, G. T.; Ma, Y. M. Reactions of Xenon with Iron and Nickel are Predicted in the Earth's Inner Core. *Nat. Chem.* **2014**, *6*, 644−648.
(30) Li, Y. W.; Hao, J.; Liu, H. Y.; Li, Y. L.; Ma, Y. M. The Metallization and Superconductivity of Dense Hydrogen Sulfide. *J. Chem. Phys.* **2014**, *140*, No. 174712.
(31) Wang, H.; Tse, J. S.; Tanaka, K.; Iitaka, T.; Ma, Y. M. Superconductive Sodalite-Like Clathrate Calcium Hydride at High Pressures. *Proc. Natl. Acad. Sci. USA* **2012**, *109*, 6463−6466.
(32) Lv, J.; Wang, Y. C.; Zhu, L.; Ma, Y. M. Predicted Novel High-Pressure Phases of Lithium. *Phys. Rev. Lett.* **2011**, *106*, No. 015503.
(33) Zhu, L.; Wang, H.; Wang, Y. C.; Lv, J.; Ma, Y. M.; Cui, Q. L.; Ma, Y. M.; Zou, G. T. Substitutional Alloy of Bi and Te at High Pressure. *Phys. Rev. Lett.* **2011**, *106*, No. 145501.
(34) Sun, W. G.; Wang, J. J.; Lu, C.; Xia, X. X.; Kuang, X. Y.; Hermann, A. Evolution of the Structural and Electronic Properties of Medium-Sized Sodium Clusters: A Honeycomb-Like Na_{20} Cluster. *Inorg. Chem.* **2017**, *56*, 1241−1248.
(35) Jin, Y. Y.; Lu, S. J.; Hermann, A.; Kuang, X. Y.; Zhang, C. Z.; Lu, C.; Xu, H. G.; Zheng, W. J. Probing the Structural Evolution of Ruthenium Doped Germanium Clusters: Photoelectron Spectroscopy and Density Functional Theory Calculations. *Sci. Rep.* **2016**, *6*, No. 30116.
(36) Xia, X. X.; Hermann, A.; Kuang, X. Y.; Jin, Y. Y.; Lu, C.; Xing, X. D. Study of the Structural and Electronic Properties of Neutral and Charged Niobium-Doped Silicon Clusters: Niobium Encapsulated in Silicon Cages. *J. Phys. Chem. C* **2016**, *120*, 677−684.
(37) Becke, A. D. Density-Functional Thermochemistry. III. The Role of Exact Exchange. *J. Chem. Phys.* **1993**, *98*, 5648−5652.
(38) Perdew, J. P.; Wang, Y. Pair-Distribution Function and its Coupling-Constant Average for the Spin-Polarized Electron Gas. *Phys. Rev. B* **1992**, *46*, 12947−12954.
(39) Perdew, J. P.; Ziesche, P.; Eschrig, H. *Electronic Structure of Solids*; Akademie Verlag: Berlin, 1991.
(40) Frisch, M. J.; Trucks, M. J.; Schlegel, H. B.; Scuseria, G. E.; Robb, M. A.; Cheeseman, J. R.; Montgomery, J. A.; Vreven, T.; Kudin, K. N.; Burant, J. C.; et al. *Gaussian 09*, revision C.0; Gaussian, Inc.: Wallingford, CT, 2009.
(41) Lu, T.; Chen, F. Multiwfn: A Multifunctional Wavefunction Analyzer. *J. Comput. Chem.* **2012**, *33*, 580−592.
(42) Huang, X. M.; Lu, S. J.; Liang, X. Q.; Su, Y.; Sai, L. W.; Zhang, Z. G.; Zhao, J. J.; Xu, H. G.; Zheng, W. J. Structures and Electronic Properties of V_3 Si_n^- (n = 3−14) Clusters: A Combined Ab Initio and Experimental Study. *J. Phys. Chem. C* **2015**, *119*, 10987−10994.
(43) Ma, L.; Zhao, J. J.; Wang, J. G.; Wang, B. L.; Lu, Q. L.; Wang, G. H. Growth Behavior and Magnetic Properties of Si_nFe (n = 2−14) Clusters. *Phys. Rev. B* **2006**, *73*, No. 125439.
(44) Kawamura, H.; Kumar, V.; Kawazoe, Y. Growth Behavior of Metal-Doped Silicon Clusters Si_nM (M = Ti, Zr, Hf; n = 8−16). *Phys. Rev. B* **2005**, *71*, No. 075423.
(45) Guo, L. J.; Zhao, G. F.; Gu, Y. Z.; Liu, X.; Zeng, Z. Density-Functional Investigation of Metal-Silicon Cage Clusters MSi_n (M = Sc, Ti, V, Cr, Mn, Fe, Co, Ni, Cu, Zn; n = 8−16). *Phys. Rev. B* **2008**, *77*, No. 195417.

DOI: 10.1021/acs.jpcc.8b09010
J. Phys. Chem. C 2019, 123, 1931−1938